Chemical Geology 280 (2011) 314–322

Contents lists available at ScienceDirect

Chemical Geology

journal homepage: www.elsevier.com/locate/chemgeo

Research paper

Identification and composition of secondary meniscus calcite in fossil coral and the effect on predicted sea surface temperature

Paul Dalbeck [a], Maggie Cusack [a,*], Phillip S. Dobson [b], Nicola Allison [c], Anthony E. Fallick [d], Alexander W. Tudhope [e] and EIMF [f]

[a] School of Geographical and Earth Sciences, Gregory Building, Lilybank Gardens, University of Glasgow, G12 8QQ, UK
[b] School of Engineering, James Watt Building, University Avenue, University of Glasgow, Glasgow, G12 8QQ, UK
[c] School of Geography and Geosciences, Irvine Building, North Street, University of St Andrews, St Andrews, Fife, KY16 9AL, UK
[d] Scottish Universities Environmental Research Centre, Rankine Avenue, East Kilbride, Glasgow, G75 0QF, UK
[e] School of Geosciences, Grant Institute, University of Edinburgh, Edinburgh EH9 3JW, UK
[f] Edinburgh Ion Microprobe Facility, School of Geosciences, Grant Institute, University of Edinburgh, Edinburgh EH9 3JW, UK

ARTICLE INFO

Article history:
Received 14 September 2010
Received in revised form 10 November 2010
Accepted 11 November 2010
Available online 28 November 2010

Editor: U. Brand

Keywords:
Meniscus calcite
Coral
Diagenesis
Sr/Ca ratio
EBSD
AFM
Biomineral

ABSTRACT

This study uses electron backscatter diffraction (EBSD) and atomic force microscopy (AFM) to identify secondary calcite in coral skeletons. Secondary calcite appears to have nucleated on the original aragonite dissepiments, producing horizontal structures that mimic the morphology of the original coral aragonite, forming dissepiment-like meniscus structures. The Sr/Ca and $\delta^{18}O$ of the pristine aragonite and secondary calcite were analysed by secondary ion mass spectrometry (SIMS). The effect of calcite inclusion on the mean geochemistry of the coral carbonate and subsequent sea surface temperature (SST) calculations were determined for both Sr/Ca and $\delta^{18}O$. Inclusion of as little as 1% secondary calcite within the primary coral aragonite elevates the Sr/Ca-derived SST by 1.2 °C and could markedly offset estimates of past tropical climate. Conversely, inclusion of 10% secondary calcite has little effect on the SST estimated from $\delta^{18}O$ (+0.6 °C) indicating that this proxy is relatively robust to even large amounts of calcite. The different extents to which the two proxies would be influenced by inadvertent inclusion of such meniscus calcite demonstrate the importance of a multi-proxy approach.

1. Introduction

Scleractinian corals produce skeletons of calcium carbonate in the form of aragonite. The chemistry of biogenic marine carbonates provides valuable geochemical information, which can be used to reconstruct past climates *via* an understanding of the interaction between the material produced and the surrounding environment. Seawater temperature at the time of coral aragonite growth can be determined using seawater temperature proxies such as $\delta^{18}O$ (Felis and Pätzold, 2003; Felis et al., 2000, 2003; Greer and Swart, 2006; Klein et al., 1992; Kuhnert et al., 1999; McConnaughey, 1989; Moses et al., 2006; Rollion-Bard et al., 2007; Swart et al., 1998, 1999) or Sr/Ca ratio (Allison and Finch, 2004; Allison et al., 2005a; Guilderson et al., 1994, 2001; Moses et al., 2006; Tudhope et al., 2001). Coral skeletal carbonate has provided a number of climate reconstructions for major features of the global climate system particularly in the South Pacific region (Charles et al., 2003; Cobb et al., 2003; Evans et al., 1998; Tudhope et al., 1996, 2001; Urban et al., 2000). However, for such reconstruction studies to be sufficiently accurate, the proxies must be reliable (Meibom et al., 2003). Coral skeletons are susceptible to alteration through diagenesis. Secondary material such as calcite and secondary aragonite can be deposited in fossil corals, adversely affecting climate estimates (Allison et al., 2007; Hendy et al., 2007; Muller et al., 2001; Nothdurft et al., 2007).

Geochemical signatures of secondary material and cements can show significant deviations from that of the original material (Allison et al., 2007; Nothdurft et al., 2007). Analysis at fine spatial resolution is therefore a necessity to avoid inclusion of secondary material in proxy calculations.

In this study we use electron backscatter diffraction (EBSD) and atomic force microscopy (AFM) to examine the crystallography of modern (pristine) and fossil (diagenetically altered) *Porites* corals. EBSD is highly effective in detecting early stages of post-mortem alteration in coral mineralogy (Cusack et al., 2008b). EBSD has become a valuable tool for providing *in situ* overviews of crystallographic orientation of polycrystalline materials and is used here to identify

* Corresponding author. Tel.: +44 141 330 5491; fax: +44 141 330 4817.
E-mail address: Maggie.Cusack@glasgow.ac.uk (M. Cusack).

0009-2541/$ – see front matter © 2010 Elsevier B.V. All rights reserved.
doi:10.1016/j.chemgeo.2010.11.018

calcite growth associated with dissepiments which are fine horizontal structures within the coral. A common feature of biogenic calcium carbonates is that they are composed of nanogranules (Cölfen and Antonietti, 2005; Cusack et al., 2008a; Dauphin, 2003; Dauphin et al., 2003; Li et al., 2004) (Cuif and Dauphin, 2005; Stolarski and Mazur, 2005). The use of AFM as a complement to EBSD analysis allows the distinction between granular, biogenic calcium carbonate and non-granular non-biogenic mineral structures (De Yoreo et al., 2007). We used secondary ion mass spectrometry (SIMS) to quantify the strontium content and stable isotopic composition of primary skeletal aragonite in a fossil (Quaternary) *Porites* coral and secondary calcite formed within the coral during diagenesis. EBSD data provides an *in situ* crystallographic context for the analysis of pristine and secondary material at a similar spatial resolution to SIMS analysis.

2. Materials and methods

2.1. Materials

A core from a living specimen of massive *Porites* sp. (cf *lutea*) coral was obtained from Jarvis Island 0°22.3′S, 159°59.0′W and a Quaternary fossil specimen was cored from a raised reef in the Huon Peninsula (Chappell, 1974) in Papua New Guinea (6°17.2063′S, 147°45.3676′E). Previous studies on cores from these specimens have detailed their environmental (Marriott et al., 2004; McCulloch et al., 1999) and geological settings (Tudhope et al., 2001).

2.2. Sample preparation

Sections of the coral cores were reduced to ~2–3 cm and mounted in epoxy resin. The resin blocks were mounted on glass thin section slides and the samples polished through a series of grinding and polishing discs. The sample surface was ground down using diamond impregnated papers at 74 μm and then 20 μm, diamond slurry at 8 μm and 6 μm followed by a compound diamond pad at 6 μm and 3 μm. Polishing stages were performed with alpha aluminium oxide at 1 μm and 0.3 μm with a final treatment with 0.06 μm colloidal silica on a short nap disc to ensure removal of any residual damaged surface layers with local stress and deformity produced during the harder compound grinding and polishing (Nowell et al., 2005; Prior et al., 1999). For EBSD, a thin carbon coat was applied (Pérez-Huerta and Cusack, 2009) to the polished slides and silver paint applied around the edges of each slide to reduce surface charge. For SIMS analyses, the polished samples were gold-coated.

2.3. Electron backscatter diffraction (EBSD)

EBSD was used to identify and characterize the crystallographic structure of areas of both fossil and modern corals. EBSD analyses were performed in an FEI Quanta 200F field emission scanning electron microscope (SEM) equipped with a TSL EBSD system running Orientation Imaging Microscopy (OIM) software version 5. EBSD and scanning electron microscopy imaging was carried out at the Imaging Spectroscopy & Analysis Centre (ISAAC) of the School of Geographical & Earth Sciences at the University of Glasgow. EBSD analyses were carried out in high vacuum mode (1.5×10^{-5} Torr) with a beam aperture of 50 μm and an accelerating voltage of 20 kV. The Kikuchi patterns were indexed using the OIM database, which contains structure files for calcite and aragonite. The structure files were tested against calcite and aragonite standard thin sections prepared using the above method of mounting and polishing. In testing the structure files, a confidence index of >0.5 and pattern fit of <2 over an average of 10 trial spot analyses was required to ensure accuracy of indexing. Hough parameters were set to a minimum peak magnitude of 2, a minimum peak distance of 19, and peak symmetry of 0.80 and a binned pattern size of 120. OIM maps were subject to two clean-up algorithm procedures to ensure that reliable data were displayed (Mahway, 2005). Grain Confidence Index (CI) Standardization was applied with a Grain Tolerance Angle of 5° and minimum grain size of 2 pixels and a Neighbour Confidence Index (CI) Correlation of CI 0.2. Further partitioning of data was applied, with only grains of CI ≥ 0.2, Fit ≤ 2.9 and IQ ≥ 19 displayed in the resultant OIM map to remove any background noise from the final data set.

2.4. Atomic force microscopy (AFM)

AFM was used to identify nano-granular biogenic carbonate and non-granular non-biogenic carbonate. Analyses were carried out in the School of Engineering at the University of Glasgow. AFM was carried out on polished and etched surfaces of coral cores. Samples were cleaned in deionised water using an ultrasonic bath for two minutes, rinsed in fresh deionised water, and then blown dry using N_2 gas. The cleaned samples were then etched for two minutes at 180 W in an O_2 plasma using a GaLa Instruments PlasmaPrep 5 barrel asher to ensure that the surface was free of contaminants. The ultrasonic water clean and N_2 dry was then repeated before a final etch for two minutes at 180 W in the barrel asher. These steps removed any residues remaining from the polishing and sputtered carbon film processes; the reduced pressure in the asher also helped to minimise any water film present on the sample surface that would be disruptive to AFM scanning. AFM imaging was carried out using Tapping mode™ on a Veeco Dimension 3000, with Nanoscope III controller, employing tapping mode silicon probes (part number OTESPAW, Veeco). AFM Tapping mode™ utilizes an oscillating tip at a tip amplitude of approximately several tens of nm when the tip is not in contact with the surface. The resolution of Tapping mode™ AFM is in the order of a few nm. Height mode analyses depict the topography of the surface. Phase imaging in AFM is a powerful extension that provides nanoscale information about surface structure that goes beyond simple topographical mapping to detect variations in chemical composition, friction and other physical properties that contribute to the viscoelastic properties of the surface (Schmitz et al., 1997). AFM images were produced using Veeco software and WSxM Scanning Probe Microscopy Software (Horcas et al., 2007), a freeware software package from Nanotec Electronica. Small sections of the coral cores were broken and mounted on aluminium stubs. These sections were gold-coated and used to acquire SEM images for an overview of the coral structure.

2.5. Secondary ion mass spectrometry (SIMS)

SIMS was used to determine the geochemistry of pristine and altered sections of the corals. Samples were gold-coated for analysis by SIMS. Areas of the coral spanning several growth lines of original skeletal material as well as secondary calcite were selected for spot analyses. Trace element ratios of the sample material were determined using a Cameca ims-4f ion microprobe with Charles Evans and Associates interface and computer control running Control-PXT v1.0 at the School of Geosciences in the University of Edinburgh. Analyses were carried out with a $^{16}O^-$ ion beam, accelerated at 14.5 kV. A primary beam current of 5 nA, an image field of 25 μm, field aperture 3 (1.8 mm) and contrast aperture 3 (150 μm) were used. An energy offset of 75 eV was applied with no evidence of any significant interference for any of the isotopes studied (Allison and Finch, 2007). Each analysis is the sum of ten cycles and, for each cycle, secondary singly-charged cations were collected at masses ^{44}Ca (2 s) and ^{88}Sr (5 s). Count rates on coral fasciculi were approximately 60,000 and 22,000 cps respectively. Internal error (the precision at a single point) was calculated from the standard deviation (σ) of Sr/Ca ratio in the ten cycles in each analysis as $2^*(\sigma/(\sqrt{10})$ and was typically 1% for Sr/Ca. Multiple analyses were performed on the carbonate standard (OKA carbonatite, Sr/Ca = 13.66 ± 1.65 mmol mol^{-1}, (representing 3

independent estimates of composition by different laboratories) to estimate relative ion yield. The accuracy of the SIMS estimates is affected by uncertainty in the composition of the standard (e.g. reflecting variations in the different OKA crystals used for SIMS and characterized by bulk analytical methods) and by potential matrix effects resulting from chemical and physical differences between the calcite standard and samples i.e. calcite and aragonite. To reduce this uncertainty, estimates of Sr/Ca have been compared along adjacent coral transects by SIMS and by bulk methods of analysis and standardization factors calculated to apply to SIMS data (Allison et al., 2005b, 2007). All the SIMS data presented here have been normalized using these factors.

Stable oxygen isotope data were acquired with a Cameca ims 1270, using a ~5 nA primary $^{133}Cs^{+}$ beam and charge compensation by a normal-incidence electron gun. Secondary ions were extracted at 10 kV, and $^{18}O^{-}$ ($\sim 8.0\times10^{6}$ cps) and $^{16}O^{-}$ ($\sim 4.0\times10^{9}$ cps) were monitored simultaneously on dual Faraday cups. Each analysis involved a pre-sputtering time of 60 s, followed by data collection in two blocks of five cycles, amounting to a total count time of 45 s. To correct for instrumental mass fractionation (IMF), all data were normalised to an internal standard, University of Wisconsin Calcite (UWC $\delta^{18}O$ 23.28 ± 0.06‰ VSMOW, J. Valley pers comm.), which was assumed to be homogeneous and was measured throughout the analytical sessions. The internal error of each analysis is +/−0.2 per mil. External error +/−0.6 per mil is shown through repeated analysis on the UWC standard of known composition. Conversion from Standard Mean Ocean Water (SMOW) to Pee Dee Belemnite (PDB) was carried out according to (Coplen et al., 1983).

2.6. Conventional mass spectrometry

Other studies have noted an offset (instrumental mass fractionation) between SIMS and conventional $\delta^{18}O$ analyses of carbonates (Rollion-Bard et al., 2003). The instrumental mass fractionation was quantified by comparing the $\delta^{18}O$ of pristine modern coral analysed by SIMS and conventional mass spectrometry. Sections of the coral specimens were screened using EBSD to ensure an absence of calcite prior to drilling. The isotopic analyses were carried out at the Scottish Universities Environmental Research Centre (SUERC) on a VG ISOCARB automated preparation system integrated with a VG ISOGAS PRISM II isotope ratio mass spectrometer. Samples between 1 and 2.5 mg were drilled out using a slow speed dental drill and transferred to a plasma asher. An oxygen plasma was set up to cold burn and remove any organic matter from the samples for 20–24 h to ensure an effective loss of organic material. A modified version of McCrea's method (McCrea, 1950) was employed to determine the $^{18}O/^{16}O$ ratio,

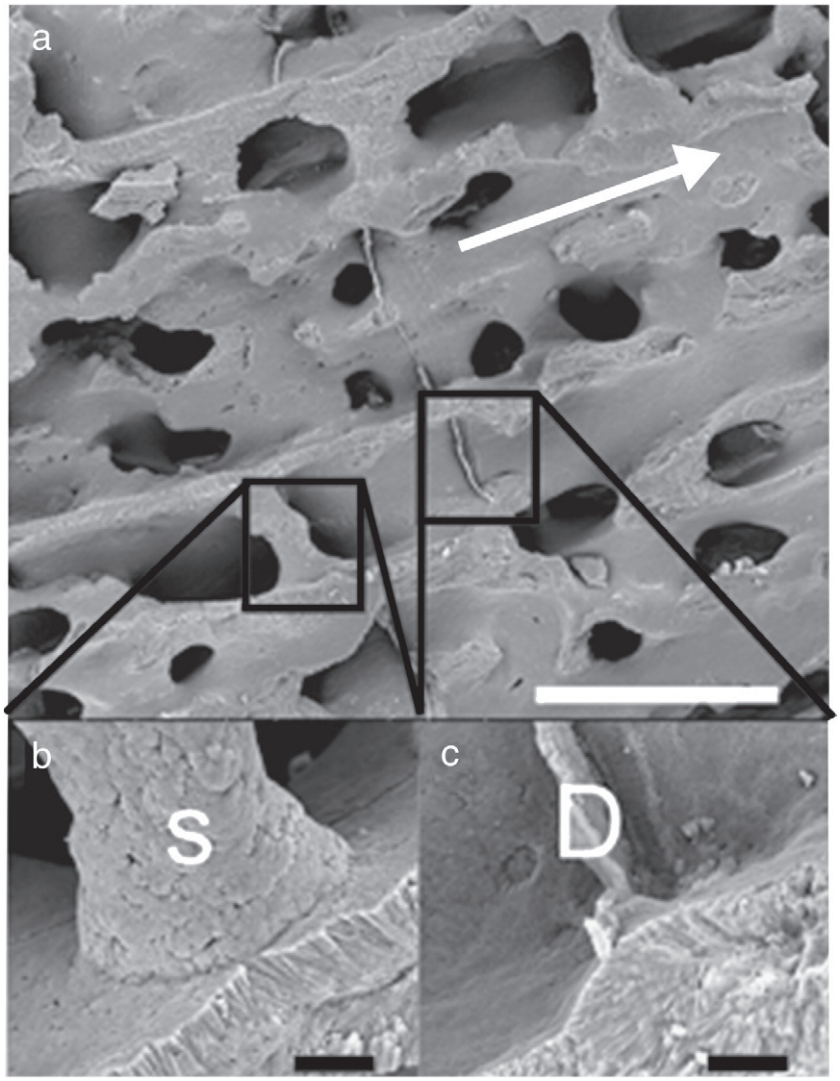

Fig. 1. Secondary electron image of fracture sections of modern *Porites lutea*. (a) Low magnification image with the direction of coral growth indicated by the white arrow. Boxed areas of horizontal structures presented in b and c. In b, a thick synapticula (S) is shown and in c, a thin dissepiment (D) is presented. In both b and c, fasciculi bundles are evident at the bottom right of both high magnification images. White scale bar in a = 500 μm, black scale bars in b and c = 20 μm.

with each sample reacted with 103% phosphoric acid (H_3PO4) at 90 °C to produce carbon dioxide (CO_2) which was then analysed. The mass spectrometer results for oxygen isotopes are corrected for isotopic fractionation between calcium carbonate and CO_2 using a fractionation factor (10^3 lnα) of 7.904 for the reaction with 103% H_3PO_4 at 90 °C. Corrections were applied using the methods similar to those described by (Craig, 1957) accounting for the presence of ^{17}O and other interference in the system. Isotopic results are reported using the conventional δ‰ notation, with reference to the Vienna Pee Dee Belemnite (VPDB) international standard (Coplen, 1995; Gonfiantini et al., 1995). Precision of each analysis was calculated through addition of internal laboratory marble (MAB2B) standards. The MAB2B laboratory standard, which is Carrara Marble, is calibrated against NBS19 and cross-checked against NBS18 and IAEA intercomparison material CO-1, CO-2 and CO-8. For each batch of analyses, reproducibility between MAB2B standards for both $^{18}O/^{16}O$ and $^{13}C/^{12}C$ was better than 0.1‰ at 1σ. Individual coral sample analyses were replicated up to three times and variability between replicate analyses was, on average, <0.3‰ at 1σ. Comparison of $\delta^{18}O$ of modern coral aragonite analysed by conventional mass spectrometry with that determined by SIMS, indicates that an offset of 2.59‰ is required to correct SIMS data. This correction has been applied to all SIMS data. Recent work suggests that the IMF may be affected by the gross trace element composition of the carbonate (Allison et al., 2010b). However there is no significant correlation between the Sr/Ca and $\delta^{18}O$ of individual SIMS analyses in a coral section indicating that the typical Sr/Ca heterogeneity observed by SIMS in coral skeletons does not affect $\delta^{18}O$ determinations (Allison et al., 2010a,b).

2.7. Estimation of surface sea temperature (SST)

Typical modern annual SST ranges at the two study sites are ~28–30 °C at the Huon Peninsula (McCulloch et al., 1999) and ~26–29 °C at Jarvis Island (Brainard et al., 2005). Modern and past SSTs were estimated from coral Sr/Ca using a palaeothermometer equation derived at Huon Peninsula (1000Sr/Ca = 10.7–0.062SST, McCulloch et al., 1999). SSTs were estimated from coral $\delta^{18}O$ assuming a typical temperature dependence of *Porites* skeletal $\delta^{18}O$ of −0.21‰ /°C (McConnaughey, 1989).

3. Results

3.1. Coral ultrastructure

Scanning electron microscopy analyses of the fossil and modern specimens reveal a typical structure of colonial scleractinian coral skeletons with long, vertical trabeculae constructed from bundles of fasciculi composed of fibrous crystals (Fig. 1). Both the thread-like dissepiments and the thicker synapticulae are visible, horizontally linking the vertical septal structures (Fig. 1).

3.2. Coral crystallography

EBSD analysis of modern coral confirms that the fasciculi crystals, radiating from the centres of calcification (COCs) are aragonite. The secondary electron images of the areas analysed by EBSD are presented in Fig. 2a and d. EBSD phase maps of these areas (Fig. 2b and e) are shown with aragonite in red and calcite in green (none present). The crystallographic orientation maps (Fig. 2c and f) show the orientation of the aragonite fibres according to the colour key in Fig. 2g.

In the fossil specimens, EBSD analysis reveals horizontal structures (Fig. 3a, d, g, and j) that can span the 200 micron gaps between septa (Fig. 3a, d, g, and j). Although they appear like dissepiments, these structures are composed of calcite as indicated in the phase maps (Fig. 3b, e, h, and k) where aragonite is in red and calcite in green.

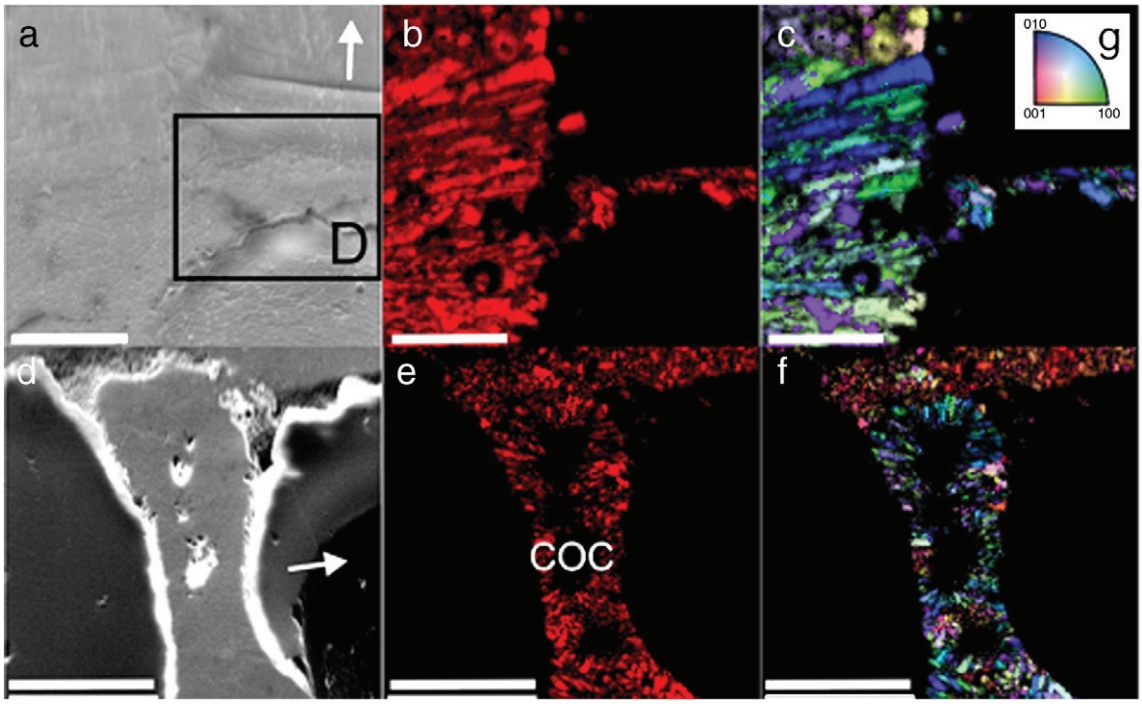

Fig. 2. Electron backscatter (EBSD) analysis of horizontal structures in modern coral. Secondary electron images (a and d) of the areas analysed by EBSD with growth direction indicated by white arrows. Box D in 2a indicates the specific area analysed in 2b and c. Phase maps (b and e) of the regions in a and d, present aragonite as red and calcite as green (none present). Crystallographic orientation maps (c and f) of the same regions indicate the crystallographic orientation of aragonite according to the colour key in g. Bundles of radiating needles of micro-crystalline aragonite comprising the main septa of the coral skeleton are evident in e and f. COC denotes the centre of calcification. Scale bar = 60 μm throughout.

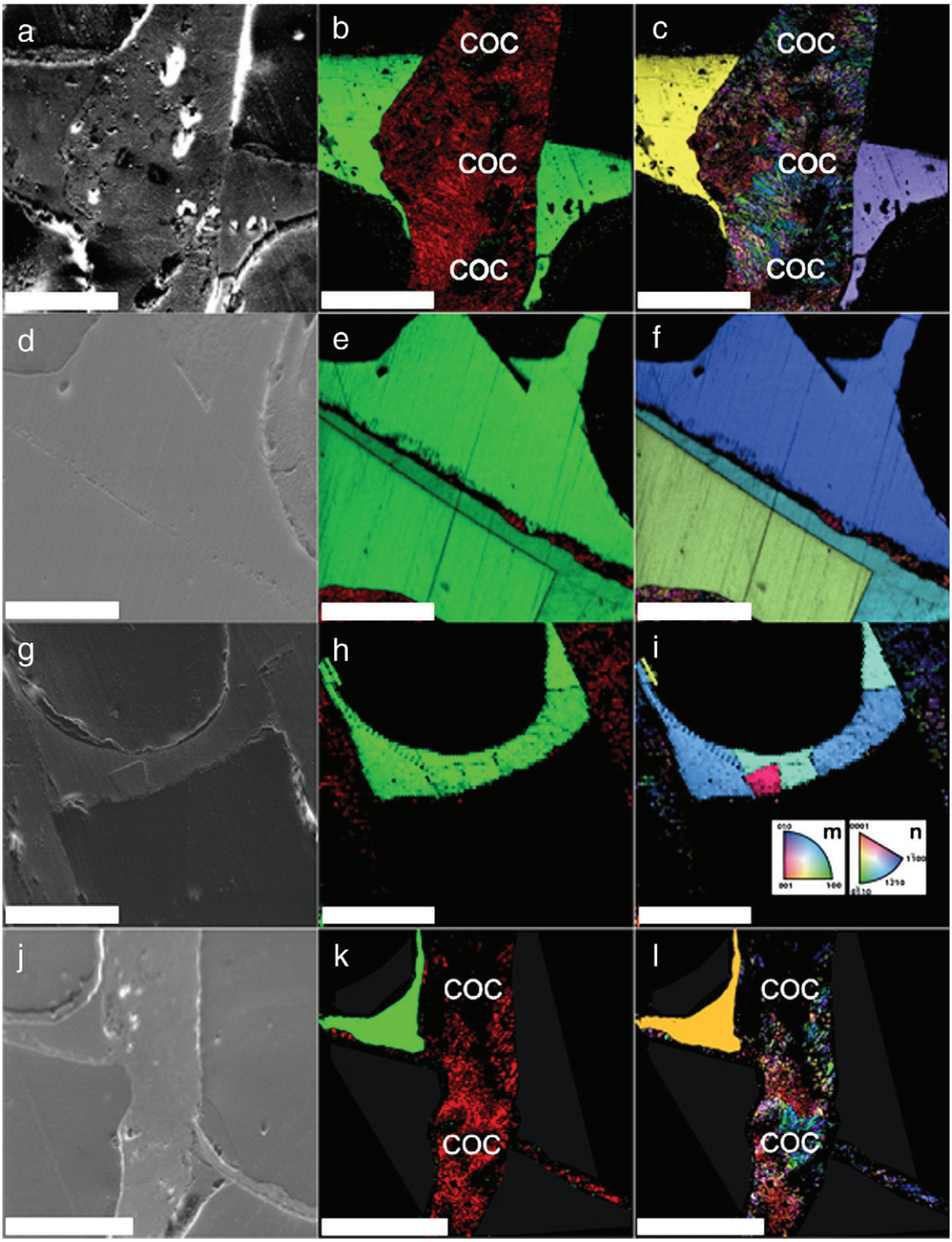

Fig. 3. Electron backscatter (EBSD) analysis of fossil coral revealing relatively large crystals of calcite resembling horizontal structures in pristine corals. Secondary electron images (a, d, g, and j) of the areas analysed by EBSD. Phase maps of these areas (b, e, h, and k) where aragonite is indicated in red and calcite in green. Crystallographic orientation maps (c, f, i, and l) of these same regions with crystallographic orientation indicated by colour key (m and n) insets in (i) for aragonite and calcite respectively. Scale Bars for a–c = 50 μm, d–f = 25 μm, g–i = 50 μm and j–l = 80 μm.

Crystallographic orientation maps (Fig. 3c, f, i, and l) indicate that the dissepiment-like structures are large, usually single crystals of calcite with crystallographic orientation indicated according to Fig. 3m, n for aragonite and calcite respectively. The bulk of the coral skeleton maintains the same crystallographic structure previously observed where the needles of aragonite radiate from the centres of calcification (COCs) (Fig. 3c and l).

3.3. Carbonate nanogranules

In the modern and fossil coral samples analysed, needles of aragonite radiate from the COCs. AFM analyses of these regions reveal that the aragonite is granular (Fig. 4a and b) indicating biogenic carbonate. Biogenic carbonate structures are composed of nanogranules surrounded by organic sheaths (Dauphin et al., 2006) with

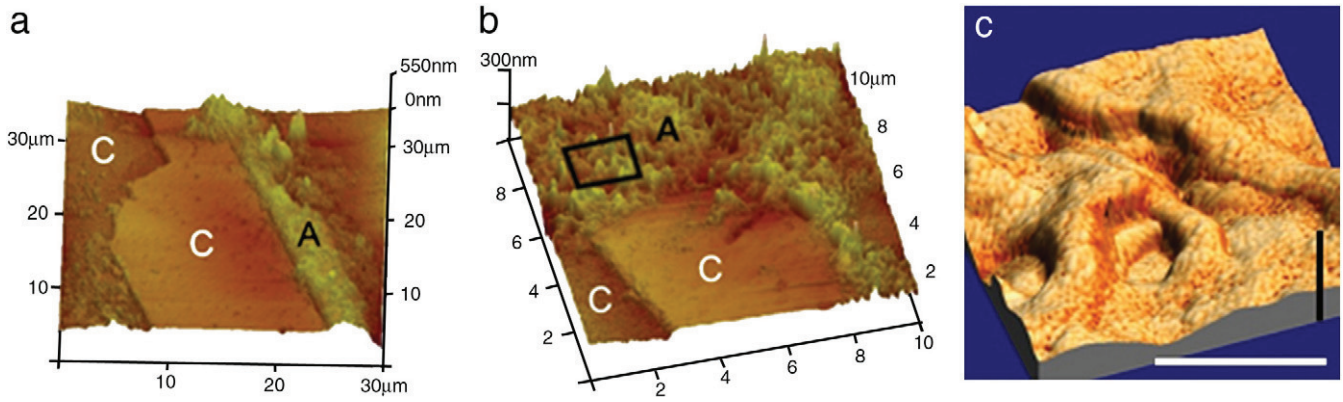

Fig. 4. Atomic force microscopy (AFM) analysis of coral aragonite and calcite in 3-D. (a) calcite 'dissepiment' (C) with a seam of aragonite (A) running through. (b) Region where the calcite makes contact with the main coral aragonite skeleton (A). (c) High magnification AFM height plot with phase overlay of the highlighted region in (b). The aragonite has a granular texture whereas the calcite is completely featureless. White scale bar = 500 nm, black vertical scale bar = 250 nm. In all cases, Z scale is height from AFM.

higher order crystals composed of nano-granules that tend to be spherules (Dauphin, 2002a; Grefsrud et al., 2008) or more triangular (Cusack et al., 2008a). These granules are also evident in fossil structures (Dauphin, 2002b). The appearance of granular aragonite in the AFM images is therefore consistent with the presence of biogenic aragonite which is an inorganic–organic composite. AFM analysis of these regions in the fossil specimens also shows flat, featureless segments of calcite contrasted against the granular texture of the aragonite (Fig. 4a–c). The lack of granules in the calcite indicates that it is likely to be a secondary structure of non-biogenic origin (Shindo and Kwak, 2005).

3.4. Strontium content

The secondary calcite in the fossil specimen has a much lower (Sr/Ca = 2.93 ± 2.10 mmol/mol, n = 36) and more variable Sr concentration than that of both the modern (Sr/Ca = 9.13 ± 0.20 mmol/mol, n = 53) and fossil (Sr/Ca = 8.98 ± 0.16 mmol/mol, n = 31) coral aragonite fibres (values are means and standard deviations (1σ)) with inevitable consequences on calculated SSTs (Fig. 5). These Sr/Ca ratios equate to estimated temperatures of 25.3 ± 3.2 °C and 27.7 ± 2.6 °C for the modern and fossil coral respectively and fall within the actual sea surface water temperature range for this region as presented in Tudhope et al. (2001). The temperature calculated from the mean Sr/Ca ratio of secondary calcite is 125.3 ± 33.9 °C (Fig. 5). Thus, with Sr/Ca as the water temperature proxy, inclusion of as little as 1% secondary calcite would elevate calculated temperatures by 1.2 °C.

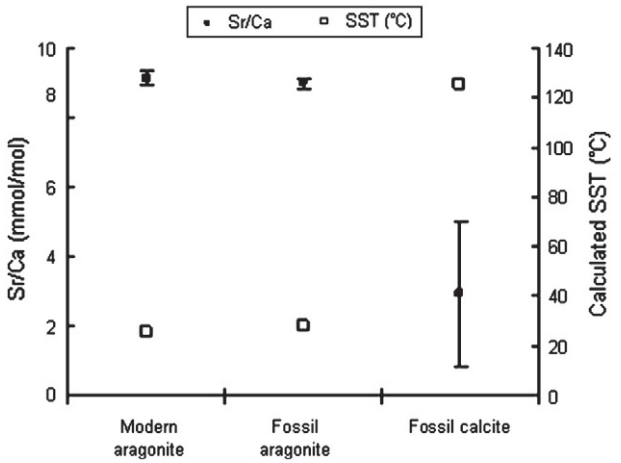

Fig. 5. Coral Sr/Ca content and calculated sea surface temperature (SST). Means and standard deviations are shown for modern coral aragonite (n = 53), fossil aragonite (n = 31) and fossil calcite (n = 36).

3.5. Isotopic difference between phases

The stable isotopic composition of modern and fossil coral aragonite was determined using conventional mass spectrometry and the sea surface temperature (SST) calculated as in Tudhope et al. (2001). $\delta^{18}O$ values of −5.26 ± 0.33 (n = 48) and −5.37 ± 0.19 (n = 24) result in calculated mean temperatures of 25.1 ± 1.6 °C and 25.6 ± 0.9 °C for modern and fossil aragonite respectively assuming a stable $\delta^{18}O_w$ (Fig. 6). The standard deviation of $\delta^{18}O$ in the pristine fossil aragonite is far larger than that observed in the drilled samples analysed by conventional mass spectrometry (Fig. 6), reflecting the $\delta^{18}O$ heterogeneity of the coral aragonite at the scale analysed by SIMS (e.g. Rollion-Bard et al., 2003). $\delta^{18}O$ of fossil calcite is lower than that of coral aragonite (Fig. 5) and equates to an estimated SST of 31.6 °C which is about 6 °C higher than would be calculated from aragonite $\delta^{18}O$ (Fig. 6). The $\delta^{18}O$ SIMS values were calculated assuming an instrumental mass fractionation (IMF) of −2.59‰. However, IMF in carbonates may be affected by trace element composition and increased from −2.1 to −2.9‰ as carbonate Sr/Ca increased from 1.2 to 9.3 mmol mol^{-1} (Allison et al., 2010a). The Sr/Ca of the secondary calcite analysed here (2.93 mmol mol^{-1}) is considerably lower than that of coral aragonite and it may be appropriate to apply a smaller IMF to this data. We are unable to calculate an exact IMF as we do not have a carbonate standard of comparable Sr/Ca to the secondary calcite. We note that applying an IMF of −2.1‰ (as

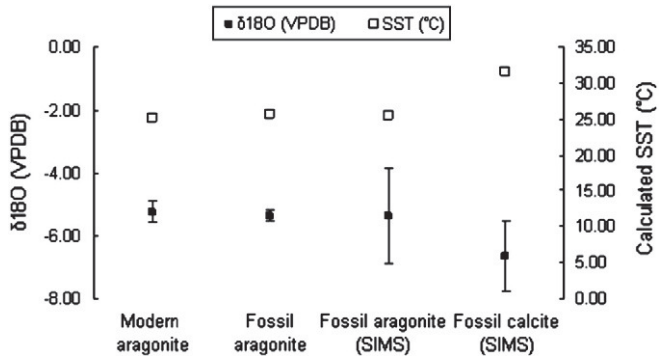

Fig. 6. $\delta^{18}O$ and calculated sea surface temperature for modern and fossil coral aragonite and fossil calcite. $\delta^{18}O$ determined for modern (n = 48) and fossil (n = 24) aragonite by conventional mass spectrometry. $\delta^{18}O$ was also determined by secondary ion mass spectrometry (SIMS) for fossil aragonite (n = 31) and calcite (n = 35). Means and standard deviations are shown.

observed in low Sr/Ca carbonates) to the SIMS analyses of the secondary calcite yields a corrected SIMS $\delta^{18}O$ of −6.1‰ and a SST estimate that is 3–4 °C higher than that calculated from the pristine coral aragonite. Thus, in this instance, $\delta^{18}O$ is much more forgiving as a water temperature proxy than Sr/Ca with inclusion of as much as 10% secondary calcite in a $\delta^{18}O$-based calculation, elevating calculated temperature by 0.6 °C.

4. Discussion

4.1. Calcite cement formation

In the fossil coral, the presence of non-biogenic calcite, that mimics the morphology of the original coral aragonite structure, has important repercussions in determining past sea surface temperature from proxy measurements. The secondary calcite appears to be nucleating on the slender horizontal aragonite dissepiments. The dissepiments, as thin shelves of material, may act as areas for pore water to be held (through capillary action and surface tension) and, as a consequence, calcite grows and assumes the form of the "meniscus" formed by the fluid held on either or both sides of the dissepiments. Fig. 7 depicts this proposed model of calcite growth on the thin dissepiments.

Meniscus cements often represent diagenetic activity in beach sands (McLaren and Gardner, 2004) in the vadose zone (McLaren, 1993). Meteoric water, undersaturated with respect to $CaCO_3$, begins to dissolve carbonate material and reprecipitates it as the more stable polymorph, calcite. The mechanism required for such large single-orientation crystals to grow remains unknown. The fact that the crystals are large suggests slow growth rate, yet the crystallographic uniformity and lack of growth zoning suggests that this non-biogenic calcite has formed in a one-off rapid event. Growth rate is likely to depend on the rate of transfer of pore fluid through the coral skeleton (Harris and Matthews, 1968). With interest surrounding the potential use of these cements as environmental indicators (Badiozamani et al., 1977; Chung and Swart, 1990), care is required in their interpretation (McLaren and Gardner, 2004). Identification and further understanding of the nature of these calcite structures may yield important palaeoclimate information recorded during diagenesis, as well as the palaeoclimate information recorded at the time of coral growth, encoded within the original coral material.

4.2. Variations in geochemistry

When the coral material is screened, prior to analysis, with EBSD it allows the identification of areas of pristine primary aragonite for high spatial resolution data acquisition. Such a selective analysis strategy is essential for reconstructing SSTs with greater accuracy from coral skeletal material (Allison et al., 2005b). The pristine aragonite analysed here shows good agreement within expected ranges in SST for data recorded for both the Jarvis Island and Huon Peninsula regions and with previous findings, for both $\delta^{18}O$ and Sr values. The observation that secondary calcite has marked differences in isotopic and geochemical composition which result in offsets in calculated temperatures from predicted SSTs reinforces previous studies that indicate that the presence of as little as 1% calcite cement can adversely affect Mg/Ca-SST estimates by as much as 11 °C (Allison et al., 2007). EBSD analyses reveal large calcite crystals in distinct regions. Indiscriminate sampling could therefore incorporate a significant portion of secondary calcite, thus affecting the gross $\delta^{18}O$ and Sr values.

An offset of 2.59‰ brings SIMS data for $\delta^{18}O$ aragonite in-line with that obtained from conventional mass spectrometry, leaving the $\delta^{18}O$ of fossil calcite noticeably lighter. Known offsets for $\delta^{18}O$ values of around 0.8‰ for calcite compared with aragonite have been reported (Grossman and Ku, 1986; Rahimpour-Bonab et al., 1997; Rye and Sommer, 1980; Tarutani et al., 1969). Such an additional adjustment has been omitted deliberately since the aim was to assess the influence of inadvertent inclusion of meniscus calcite into proxy calculations given the fact that the meniscus calcite appears original due to the mode of formation and could therefore slip through screening procedures. Likewise, no attempt was made to apply equations specific for calcite that would allow for difference in behaviour between calcite and aragonite polymorphs (Gaetani and Cohen, 2004, 2006; Kinsman and Holland, 1969; Mucci et al., 1989; Rahimpour-Bonab et al., 1997; Zhong and Mucci, 1989).

The impact of the inclusion of meniscus calcite on sea surface temperature calculations depends on the amount of material included. The values presented in Figs. 5 and 6 for 100% meniscus calcite should be easy to spot. Secondary meniscus calcite is a minor component and we estimate that it accounts for less than 1% of the calcium carbonate present. The real danger arises from inclusion of smaller quantities that may increase calculated temperatures to values that appear reasonable even if they are wrong. The extent of impact also depends on which proxy is applied with a smaller increase in calculated temperature occurring with $\delta^{18}O$ (Fig. 6) compared to the major elevation in calculated SST that could occur by applying the Sr/Ca ratio as the proxy of choice (Fig. 5). Inclusion of 10% calcite within a coral sample elevates the Sr/Ca-derived SST by 12.5 °C, but has little effect on the SST estimated from $\delta^{18}O$ (+0.3–0.6 °C, depending on IMF used). The fact that $\delta^{18}O$ and Sr/Ca are influenced to different extents by the inclusion of meniscus calcite may simply result from the specific environment in which the secondary calcite formed in this case. The difference in proxy response supports a multi-proxy approach where such discrepancies would be revealed.

Corals are an important tool in the reconstruction of past climates and this study reinforces recent reports stressing the need for careful

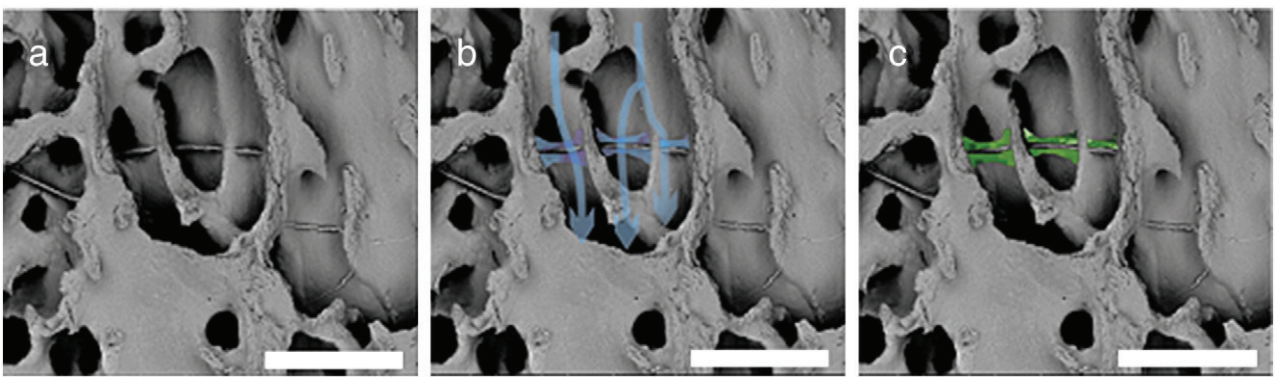

Fig. 7. Diagram representing the formation of 'meniscus' secondary calcite cement within the coral structure. (a) Primary, unaltered sample showing slender, horizontal aragonite dissepiments. (b) Arrows indicate pore water running through the sample, with some water being held on imperfections by capillary action and surface tension. (c) Calcite (green) is deposited on the aragonite dissepiments with the new crystals assuming the form of the water meniscus. Scale bar = 400 μm.

sampling and improvements in sample screening of coral material prior to analysis (Allison et al., 2005a, 2007; Nothdurft et al., 2007). The secondary calcite observed in this study mimics morphological structures of the original aragonite skeletal material and yields distinct anomalies in geochemistry when analysed at high spatial resolution. These compositional anomalies result in large offsets in calculated SST and thus, deliberate steps are required to avoid inclusion of such material in SST calculations, ensuring that only pristine, original material is selected for climate proxy studies.

Acknowledgements

The authors all gratefully acknowledge financial support from the Leverhulme Trust (F/100179/X) and the UK Natural Environment Research Council (NER/T/S2002/00443 and GR3/12021). Peter Chung is thanked for his help in scanning electron microscopy and electron backscatter diffraction. We thank John Gilleece for his help with sample preparation. Andy Freer is thanked for his constructive comments on the text. This work is in keeping with the aims of Theme 3 of the Scottish Alliance for Geoscience, Environment and Society (SAGES).

Appendix A. Supplementary data

Supplementary data to this article can be found online at doi:10.1016/j.chemgeo.2010.11.018.

References

Allison, N., Finch, A.A., 2004. High-resolution Sr/Ca records in modern *Porites lobata* corals: effects of skeletal extension rate and architecture. Geochemistry, Geophysics, Geosystems 5, Q05001. doi:10.1029/2004GC000696.

Allison, N., Finch, A.A., 2007. High temporal resolution Mg/Ca and Ba/Ca records in modern *Porites lobata* corals. Geochemistry, Geophysics, Geosystems 8, Q05001. doi:10.1029/2006GC001477.

Allison, N., Finch, A.A., Newville, M., Sutton, S.R., 2005a. Strontium in coral aragonite: 3. Sr coordination and geochemistry in relation to skeletal architecture. Geochimica et Cosmochimica Acta 69 (15), 3801–3811.

Allison, N., Finch, A.A., Tudhope, A.W., Newville, M., Sutton, S.R., Ellam, R.M., 2005b. Reconstruction of deglacial sea surface temperatures in the tropical Pacific from selective analysis of a fossil coral. Geophysical Research Letters 32 (17), L17609. doi:10.1029/2005GL023183.

Allison, N., Finch, A.A., Webster, J.M., Clague, D.A., 2007. Palaeoenvironmental records from fossil corals: the effects of submarine diagenesis on temperature and climate estimates. Geochimica et Cosmochimica Acta 71 (19), 4693–4703.

Allison, N., Finch, A.A., EIMF, 2010a. The potential origins and palaeoenvironmental implications of high temporal resolution $\delta^{18}O$ heterogeneity in coral skeletons. Geochimica et Cosmochimica Acta 74, 5537–5548.

Allison, N., Finch, A.A., EIMF, 2010b. $\delta^{11}B$, Sr, Mg and B in a modern Porites coral: the relationship between calcification site pH and skeletal chemistry. Geochimica et Cosmochimica Acta 74 (6), 1790–1800.

Badiozamani, K., Mackenzie, F.T., Thorstenson, D.C., 1977. Experimental carbonate cementation — salinity, temperature and vadose-phreatic effects. Journal of Sedimentary Petrology 47 (2), 529–542.

Brainard, R.B., Maragos, J., Schroeder, R., Kenyon, J.C., Vroom, P.S., Godwin, S., Hoeke, R.K., Aeby, G.S., Moffitt, R., Lammers, M., Gove, J., Timmers, M., Holzwarth, S.R., Kolinski, S., 2005. The state of coral reef ecosystems of the Pacific Remote Island Areas. In: Waddell, J.E. (Ed.), The state of coral reef ecosystems of the United States and Pacific Freely Associated States. NOAA Technical Memorandum NOS NCCOS 11. NOAA/NCCOS Center for Coastal Monitoring and Assessment's Biogeography Team, pp. 338–372.

Chappell, J., 1974. Geology of coral terraces, Huon-Peninsula, New-Guinea — study of Quaternary tectonic movements and sea-level changes. Geological Society of America Bulletin 85 (4), 553–570.

Charles, C.D., Cobb, K.M., Moore, M.D., Fairbanks, R.G., 2003. Monsoon-tropical ocean interaction in a network of coral records spanning the 20th century. Marine Geology 201, 207–222.

Chung, G.S., Swart, P.K., 1990. The concentration of uranium in fresh-water vadose and phreatic cements in a Holocene ooid cay — a method of identifying ancient water tables. Journal of Sedimentary Petrology 60 (5), 735–746.

Cobb, K.M., Charles, C.D., Cheng, H., Edwards, R.L., 2003. El Nino/Southern Oscillation and tropical Pacific climate during the last millennium. Nature 424, 271–276.

Cölfen, H., Antonietti, M., 2005. Mesocrystals: inorganic superstructures made by highly parallel crystallization and controlled alignment. Angewandte Chemie. International Edition 44 (35), 5576–5591.

Coplen, T.B., 1995. Discontinuance of SMOW and PDB. Nature 375 (6529), 285.

Coplen, T.B., Kendall, C., Hopple, J., 1983. Comparison of stable isotope reference samples. Nature 302, 236–238 (London, United Kingdom).

Craig, H., 1957. Isotopic standards for carbon and oxygen and correction factors for mass-spectrometric analysis pf carbon dioxide. Geochimica et Cosmochimica Acta 12 (1–2), 133–149.

Cuif, J.P., Dauphin, Y., 2005. The two-step mode of growth in the Scleractinian coral skeletons from the micrometre to the overall scale. Journal of Structural Biology 150 (3), 319–331.

Cusack, M., Dauphin, Y., Chung, P., Pérez-Huerta, A., Cuif, J.P., 2008a. Multiscale structure of calcite fibres of the shell of the brachiopod *Terebratulina retusa*. Journal of Structural Biology 164, 96–100.

Cusack, M., England, J., Dalbeck, P., Tudhope, A.W., Fallick, A.E., Allison, N., 2008b. Electron Backscatter Diffraction (EBSD) as a tool for detection of coral diagenesis. Coral Reefs 27 (4), 905–911.

Dauphin, Y., 2002a. Fossil organic matrices of the Callovian aragonitic ammonites from Lukow (Poland): location and composition. International Journal of Earth Sciences 91 (6), 1071–1080.

Dauphin, Y., 2002b. Structures, organo–mineral compositions and diagenetic changes in biominerals. Current Opinion in Colloid and Interface Science 7, 133–138.

Dauphin, Y., 2003. Soluble organic matrices of the calcitic prismatic shell layers of two pteriomorphid bivalves — *Pinna nobilis* and *Pinctada margaritifera*. The Journal of Biological Chemistry 278 (17), 15168–15177.

Dauphin, Y., Guzman, N., Denis, A., Cuif, J.P., Ortlieb, L., 2003. Microstructure, nanostructure and composition of the shell of *Concholepas concholepas* (Gastropoda, Muricidae). Aquatic Living Resources 16 (2), 95–103.

Dauphin, Y., Cuif, J.P., Massard, P., 2006. Persistent organic components in heated coral aragonitic skeletons — implications for palaeoenvironmental reconstructions. Chemical Geology 231 (1–2), 26–37.

De Yoreo, J.J., Wierzbicki, A., Dove, P.M., 2007. New insights into mechanisms of biomolecular control on growth of inorganic crystals. Crystengcomm 9, 1144–1152.

Evans, M.N., Fairbanks, R.G., Rubenstone, J.L., 1998. A proxy index of ENSO teleconnections. Nature 394 (6695), 732–733.

Felis, T., Pätzold, J., 2003. Climate records from corals. In: Wefer, G., Lamy, F., Mantoura, F. (Eds.), Marine Science Frontiers for Europe. Springer-Verlag, Berlin, pp. 11–27.

Felis, T., Pätzold, J., Loya, Y., Fine, M., Nawar, A.H., Wefer, G., 2000. A coral oxygen isotope record from the northern Red Sea documenting NAO, ENSO, and north Pacific teleconnections on Middle East climate variability since the year 1750. Paleoceanography 15, 679–694.

Felis, T., Pätzold, J., Loya, Y., 2003. Mean oxygen-isotope signatures in Porites sp. corals: inter-colony variability and correction for extension-rate effects. Coral Reefs 22, 328–336.

Gaetani, G.A., Cohen, A.L., 2004. Experimental investigation of the partitioning of Mg^{2+}, Ca^{2+}, Sr^{2+}, and Ba^{2+} between aragonite and seawater at 5 to 45 °C. Geochimica et Cosmochimica Acta 68 (11), A209.

Gaetani, G.A., Cohen, A.L., 2006. Element partitioning during precipitation of aragonite from seawater: a framework for understanding paleoproxies. Geochimica et Cosmochimica Acta 70 (18), 4617–4634.

Gonfiantini, R., Stichler, W., Rozanski, K., 1995. Standards and intercomparison materials distributed by the International Atomic Energy Agency for stable isotope measurements. Reference and Intercomparison Materials for Stable Isotopes of Light Elements. International Atomic Energy Agency, Vienna, pp. 13–29.

Greer, L., Swart, P.K., 2006. Decadal cyclicity of regional mid-Holocene precipitation: evidence from Dominican coral proxies. Paleoceanography 21 (2). doi:10.1029/2005PA001166.

Grefsrud, E.S., Dauphin, Y., Cuif, J.P., Denis, A., Strand, O., 2008. Modifications in microstructure of cultured and wild scallop shells (Pecten maximus). Journal of Shellfish Research 27 (4), 633–641.

Grossman, E.L., Ku, T.-L., 1986. Oxygen and carbon isotope fractionation in biogenic aragonite: temperature effects. Chemical Geology 59, 59–74.

Guilderson, T.P., Fairbanks, R.G., Rubenstone, J.L., 1994. Tropical temperature-variations since 20, 000 years ago — modulating interhemispheric climate-change. Science 263 (5147), 663–665.

Guilderson, T.P., Fairbanks, R.G., Rubenstone, J.L., 2001. Tropical Atlantic coral oxygen isotopes: glacial–interglacial sea surface temperatures and climate change. Marine Geology 172 (1–2), 75–89.

Harris, W.H., Matthews, R.K., 1968. Subaerial diagenesis of carbonate sediments: efficiency of the solution-reprecipitation process. Science 160, 77–79.

Hendy, E.J., Gagan, M.K., Lough, J.M., McCulloch, M., deMenocal, P.B., 2007. Impact of skeletal dissolution and secondary aragonite on trace element and isotopic climate proxies in *Porites* corals. Paleoceanography 22, PA4101. doi:10.1029/2007PA001462.

Horcas, I., Fernandez, R., Gomez-Rodriguez, J.M., Colchero, J., Gomez-Herrero, J., Baro, A.M., 2007. WSXM: a software for scanning probe microscopy and a tool for nanotechnology. The Review of Scientific Instruments 78 (1), 013705–013708.

Kinsman, D.J.J., Holland, H.D., 1969. Co-precipitation of cations with $CaCO_3$ IV. Co-precipitation of Sr^{2+} with aragonite between 16 and 96 °C. Geochimica et Cosmochimica Acta 33 (1), 1–18.

Klein, R., Pätzold, J., Wefer, G., Loya, Y., 1992. Seasonal variations in the stable isotopic composition and the skeletal density pattern of the coral *Porites lobata*, Gulf of Eilat, Red Sea. Marine Biology 112, 259–263.

Kuhnert, H., Pätzold, J., Hatcher, B., Wyrwoll, K.H., Eisenhauer, A., Collins, L.B., Zhu, Z.R., Wefer, G., 1999. A 200-year coral stable oxygen isotope record from a high-latitude reef off western Australia. Coral Reefs 18, 1–12.

Li, X.D., Chang, W.C., Chao, Y.J., Wang, R.Z., Chang, M., 2004. Nanoscale structural and mechanical characterization of a natural nanocomposite material: the shell of red abalone. Nano Letters 4 (4), 613–617.

Mahway, E., 2005. OIM User's Manual. EDAX-TSL, New Jersey.
Marriott, C.S., Henderson, G.M., Crompton, R., Staubwasser, M., Shaw, S., 2004. Effect of mineralogy, salinity, and temperature on Li/Ca and Li isotope composition of calcium carbonate. Chemical Geology 212 (1–2), 5–15.
McConnaughey, T., 1989. ^{13}C and ^{18}O isotopic disequilibrium in biological carbonates. 2. *In vitro* simulation of kinetic isotope effects. Geochimica et Cosmochimica Acta 53 (1), 163–171.
McCrea, J.M., 1950. On the isotopic chemistry of carbonates and a paleotemperature scale. The Journal of Chemical Physics 18 (6), 849–857.
McCulloch, M.T., Tudhope, A.W., Esat, T.M., Mortimer, G.E., Chappell, J., Pillans, B., Chivas, A.R., Omura, A., 1999. Coral record of equatorial sea-surface temperatures during the penultimate deglaciation at Huon Peninsula. Science 283 (5399), 202–204.
McLaren, S.J., 1993. Use of cement types in the palaeoenvironmental interpretation of coastal aeolianite sequences. In: Pye, K. (Ed.), The Dynamics and Environmental Context of Aeolian Sedimentary Systems. Geological Society Special Publication, pp. 235–244.
McLaren, S.J., Gardner, R.A.M., 2004. Late Quaternary vadose carbonate diagenesis in coastal and desert dune and beach sands: is there a palaeoclimatic signal? Earth Surface Processes and Landforms 29, 1441–1458.
Meibom, A., Stage, M., Wooden, J., Constantz, B.R., Dunbar, R.B., Owen, A., Grumet, N., Bacon, C.R., Chamberlain, C.P., 2003. Monthly strontium/calcium oscillations in symbiotic coral aragonite: biological effects limiting the precision of the paleotemperature proxy. Geophysical Research Letters 30 (7).
Moses, C.S., Swart, P.K., Dodge, R.E., 2006. Calibration of stable oxygen isotopes in Siderastrea radians (Cnidaria: Scleractinia): implications for slow-growing corals. Geochemistry, Geophysics, Geosystems 7.
Mucci, A., Canuel, R., Zhong, S.J., 1989. The solubility of calcite and aragonite in sulfate-free seawater and the seeded growth-kinetics and composition of the precipitates at 25-degrees-C. Chemical Geology 74 (3–4), 309–320.
Muller, A., Gagan, M.K., McCulloch, M.T., 2001. Early marine diagenesis in corals and geochemical consequences for paleoceanographic reconstructions. Geophysical Research Letters 28, 4471–4474.
Nothdurft, L.D., Webb, G.E., Bostrom, T., Rintoul, L., 2007. Calcite-filled borings in the most recently deposited skeleton in live-collected *Porites* (Scleractinia): implications for trace element archives. Geochimica et Cosmochimica Acta 71 (22), 5423–5438.
Nowell, M.M., Witt, R.A., True, B., 2005. EBSD sample preparation: techniques tips and tricks. Microscopy and Microanalysis 11, 504–505.
Pérez-Huerta, A., Cusack, M., 2009. Optimising electron backscatter diffraction (EBSD) of carbonate biominerals — resin type and carbon coating. Microscopy and Microanalysis 15, 197–203.
Prior, D.J., Boyle, A.P., Brenker, F., Cheadle, M.C., Day, A., Lopez, G., Peruzzo, L., Potts, G.J., Reddy, S., Spiess, R., Timms, N.E., Trimby, P., Wheeler, J., Zetterstrom, L., 1999. The application of electron backscatter diffraction and orientation contrast imaging in the SEM: the textural problems. American Mineralogist 84, 1741–1759.
Rahimpour-Bonab, H., Bone, Y., Moussavi-Harami, R., 1997. Stable isotope aspects of modern molluscs, brachiopods, and marine cements from cool-water carbonates, Lacepede Shelf, South Australia. Geochimica et Cosmochimica Acta 61 (1), 207–218.
Rollion-Bard, C., Blamart, D., Cuif, J.P., Juillet-Leclerc, A., 2003. Microanalysis of C and O isotopes of azooxanthellate and zooxanthellate corals by ion microprobe. Coral Reefs 22 (4), 405–415.
Rollion-Bard, C., Blamart, D., Cuif, J.P., Meibom, A., Juillet-Leclerc, A., Dauphin, Y., 2007. Oxygen isotopic composition in deep-sea coral, *Lophelia pertusa*. Geochimica et Cosmochimica Acta 71 (15), 849.
Rye, D.M., Sommer, M.A., 1980. Reconstructing paleotemperature and paleosalinity regimes with oxygen isotopes. In: Rhoads, D.C., Lutz, R.A. (Eds.), Skeletal Growth of Aquatic Organisms. Plenum Press, New York, pp. 169–202.
Schmitz, I., Schreiner, M., Friedbacher, G., Grasserbauer, M., 1997. Phase imaging as an extension to tapping mode AFM for the identification of material properties on humidity-sensitive surfaces. Applied Surface Science 155, 190–198.
Shindo, H., Kwak, M., 2005. Stabilities of crystal faces of aragonite ($CaCO_3$) compared by atomic force microscopic observation of facet formation processes in aqueous acetic acid. Physical Chemistry Chemical Physics 7 (4), 691–696.
Stolarski, J., Mazur, M., 2005. Nanostructure of biogenic versus abiogenic calcium carbonate crystals. Acta Palaeontologica Polonica 50 (4), 847–865.
Swart, P.K., White, K.S., Enfield, D., Dodge, R.E., Milne, P., 1998. Stable oxygen isotopic composition of corals from the Gulf of Guinea as indicators of periods of extreme precipitation conditions in the sub-Sahara. Journal of Geophysical Research, Oceans 103 (C12), 27885–27891.
Swart, P.K., Healy, G., Greer, L., Lutz, M., Saied, A., Anderegg, D., Dodge, R.E., Rudnick, D., 1999. The use of proxy chemical records in coral skeletons to ascertain past environmental conditions in Florida Bay. Estuaries 22 (2B), 384–397.
Tarutani, T., Clayton, R.N., Mayeda, T.K., 1969. Effect of polymorphism and magnesium substitution on oxygen isotope fractionation between calcium carbonate and water. Geochimica et Cosmochimica Acta 33 (8), 987–996.
Tudhope, A.W., Shimmield, G.B., Chilcott, C.P., Jebb, M., Fallick, A.E., Dalgleish, A.N., 1995. Recent changes in climate in the far western equatorial Pacific and their relationship to the Southern Oscillation; oxygen isotope records from massive corals, Papua New Guinea. Earth and Planetary Science Letters 136 (3–4), 575–590.
Tudhope, A.W., Lea, D.W., Shimmield, G.B., Chilcott, C.P., Head, S., 1996. Monsoon climate and Arabian sea coastal upwelling recorded in massive corals from southern Oman. Palaios 11 (4), 347–361.
Tudhope, A.W., Chilcott, C.P., McCulloch, M.T., Cook, E.R., Chappell, J., Ellam, R.M., Lea, D.W., Lough, J.M., Shimmield, G.B., 2001. Variability in the El Nino — southern oscillation through a glacial–interglacial cycle. Science 291 (5508), 1511–1517.
Urban, F.E., Cole, J.E., Overpeck, J.T., 2000. Influence of mean climate change on climate variability from a 155-year tropical Pacific coral record. Nature 407 (6807), 989–993.
Zhong, S.J., Mucci, A., 1989. Calcite and aragonite precipitation from seawater solutions of various salinities — precipitation rates and overgrowth compositions. Chemical Geology 78 (3–4), 283–299.